Hindawi
Geofluids
Volume 2019, Article ID 1967080, 15 pages
https://doi.org/10.1155/2019/1967080

Research Article

Study on Deformation and Permeation Properties of Gas-Containing Fractured Rock

Yushun Yang[1,2] **Dongming Zhang**[1,2] **and Shujian Li**[1,2]

[1]*State Key Laboratory of Coal Mine Disaster Dynamics and Control, Chongqing University, Chongqing 400044, China*
[2]*College of Resources and Environmental Science, Chongqing University, Chongqing 400044, China*

Correspondence should be addressed to Dongming Zhang; zhangdm@cqu.edu.cn

Received 18 December 2018; Revised 29 March 2019; Accepted 17 April 2019; Published 25 June 2019

Academic Editor: Andri Stefansson

In this paper, we investigated the gas permeation properties of fractured rock during the process of stage load axial stress and cyclic load and unload confining pressure and come to some conclusions as follows: (1) the relationship between radial strain and deviatoric stress satisfied the quadratic polynomial function, and the relationship between permeability and deviatoric stress satisfied the exponential function under different axial stress levels; (2) in the staged load axial stress process, the axial strain-deviatoric curves of specimens conform to the quadratic polynomial function. The axial strain-deviatoric curves of specimens conform to linear function when confining pressure is 8.6 MPa or 2.0 MPa at different axial stress levels; (3) we used the permeability damage rate and maximum permeability damage rate to evaluate the recovery degree and reduction extent of permeability; (4) we used the volume expansion ratio and the maximum volume expansion ratio to evaluate the expansion degree and increase extent of rock samples' volume.

1. Introduction

In the underground mining process, the coal body affected by mining has multiple distributions of stress field, which leads to constant abutment stress or pressure relief area in the mining process, while the roof strata of the goaf are broken and undergo a repeated loading and unloading process. The gas in the coal seam migrates upward and accumulates along the fractured rock mass of the coal seam roof, which easily causes a gas outburst accident [1]. Therefore, it is important to investigate the deformation and permeability of fractured rock.

Many researches have been done for the mechanic properties of coal-rock in recent years. It is considered that confining pressure and pore pressure affect rock permeability in different degrees [2–5], the change of rock permeability can be explained by effective stress principle, and a damage model was proposed based on micromechanics to describe the anisotropic damage characteristics of rock samples [6]. The test results show that the permeability of brittle rock increases rapidly at a critical failure point [7], while the mechanical and permeability characteristics of sandstone and limestone are different before and after failure [8]. Zhao et al. [9] conducted the model of the logical fracture behavior of rock cracks subjected to hydraulic pressure and far field stresses. In view of the creep-seepage coupling characteristics of rock, the variation of seepage velocity with time in the process of complete creep of rock was analyzed [10], the permeability characteristics of clay rock during a triaxial creep process were discussed [11], and the creep, permeability variation, and seepage-creep coupling mechanism of rocks were discussed during the loading and unloading process [12]. According to the cyclic loading and unloading test of rock specimens, the permeability evolution law of sandstone specimens in the whole process of failure was analyzed [13], and the relationship between the damage evolution and permeability of granite specimens is also analyzed [14]. Zhao et al. [15] conducted extensive laboratory investigation of the nonlinear rheological mechanical characteristics of hard rock under cyclic incremental loading and unloading and proposed a data processing algorithm to analyze the experimental data. According to the sandstone specimen test, the

variation of permeability with axial strain, radial strain, and volumetric strain was analyzed in the process of complete stress-strain curves [16] and established the gas seepage model of a strain index and the effect of stress concentration state on the deformation law and seepage characteristics of sandstone in the process of unloading confining pressure failure [17, 18]. Huang and Hu [19] investigated the damage of shale rock impacted by a high-pressure supercritical carbon dioxide (SC-CO_2) jet and used a well-designed apparatus to conduct experiments with a high-pressure SC-CO_2 jet impacting shale core plugs. A rough single-fracture sandstone seepage model based on dimensional analysis is established for the fracture seepage test of rough single-fractured sandstone specimens [20]. Huang et al. [21] investigated the lateral jetting commencing points associated with the peak pressure when an arc-curved jet impacts flat, concave, convex, and inclined solid surfaces, respectively. Temperature and water content have different effects on rock permeability. It is considered that the permeability coefficient increases with temperature. For a given temperature level, the transmittance decreases with the increase of confining pressure, and the decline rate decreases gradually [22]. The interaction between physical properties, volume change, and permeability of hard sandstone under complete water saturation is described [23]. Zhao et al. [24] performed the transient pulse tests on single rock fractures at different confining pressures, and a new data analysis method based on polynomial fitting was introduced to investigate the relationship between flow velocity and hydraulic gradient.

Previous studies mainly focused on the mechanics and permeability of intact coal and rock, and there is little research on the deformation and permeability of fractured rock. During the mining process of the working face, the roof rock is deformed and broken, and then, the fractured rock mass is formed. The gas inside the coal seam migrates to the goaf and along the crack to the top of the rock stratum. Therefore, the study of gas migration in fractured rock mass during the loading and unloading process is of great significance for the treatment of coal and gas outbursts.

2. Specimens, Equipment, and Methods

Rock samples come from the roof of coal seam #2+3 of the Yibin coal field in Sichuan, China. Several cuboid rock samples measuring 100 mm × 100 mm × 150 mm were cut into the appropriate size of 50 mm diameter and 100 mm length for triaxial seepage tests. A thermal-fluid-solid coupling triaxial servo seepage device developed (Chongqing University, Chongqing, China) [25] was employed to conduct the triaxial seepage tests, as shown in Figure 1. The equipment can conduct a coal-rock gas permeability test under different stresses and gas pressure. The maximum axial pressure is 200 kN, the confining pressure is 10 MPa, the maximum axial deformation displacement is 60 mm, and the maximum radial deformation is 6 mm. The temperature ranges from room temperature to 100°C. The stress measurement system has an accuracy of ±1%, a deformation accuracy of ±1%, and a temperature control accuracy of ±1%.

During the coal seam mining process, the stress changes complexly in front of the working face and appears on the stress concentration zone, the stress reduction zone, and the original stress zone. The overburdened strata in the goaf are broken; the roof falls and undergoes a complex loading and unloading process. Therefore, it is of great significance to study the mechanical and permeability characteristics of fractured rock samples during the loading and unloading process to prevent and control coal and gas outbursts. Load and unload seepage tests on specimens damaged by triaxial compression, that is, loading axial stress at stage and cyclic loading and unloading confining pressure test of fractured rock, are as follows: (1) gradually apply $\sigma_1 = \sigma_2(\sigma_3)$ to a hydrostatic pressure of 2 MPa; (2) keep the gas pressure at 0.5 MPa; (3) keep the gas fully absorbed for 12 h until reaching equilibrium; (4) load axial stress of 4 MPa, 6 MPa, 8 MPa, 10 MPa, 12 MPa, 14 MPa, 16 MPa, 18 MPa, and 20 MPa at the stress control loading rate of 0.05 kN/s at stage. Under different axial stress stages, load confining pressure of 8.6 MPa at a loading rate of 0.05 MPa/s, then unload confining pressure of 2.0 MPa at the same rate; (5) maintain 2 MPa confining pressure constant and load axial stress till fractured rock failure at displacement control loading rate of 0.1 mm/min. There are 3 fractured rock specimens of #j_1, #j_2, and #j_3 in this seepage test.

3. Results and Discussion

Assuming that the gas flow in the fractured rock conforms to Darcy's law, the permeability of fractured rock was continuously calculated by [18, 25]

$$k = \frac{2v\mu L p_2}{S\left(p_1^2 - p_2^2\right)}, \tag{1}$$

where k presents the permeability (mD), v is gas seepage velocity (cm^3/s), μ refers to the gas kinematic viscosity (Pa·s), L is the length of fractured rock (mm), S is the cross-section area of fractured rock (mm^2), p_1 is gas pressure at the sample inlet (MPa), and p_2 is gas pressure at the sample outlet (MPa).

3.1. Analysis of Deformation and Permeability Properties. The complete stress-strain-permeability curves of fractured rock under load and unload conditions are presented in Figure 2.

We can see from Figure 2 that the permeability of each sample fluctuates greatly; this is because this is related to the test scheme designed in this paper. Specific test schemes are load axial stress of 4 MPa, 6 MPa, 8 MPa, 10 MPa, 12 MPa, 14 MPa, 16 MPa, 18 MPa, and 20 MPa at a stress control loading rate of 0.05 kN/s at stage. When the axial pressure is loaded to the preset stress level, constant axial stress and loading-unloading confining pressure tests are carried out. The permeability decreases nonlinearly in the process of loading confining pressure but increases nonlinearly in the process of unloading confining pressure. Therefore, the permeability of the sample shows big fluctuations.

Details are observed in Figure 2, while maintaining confining pressure constant and load axial stress process, the

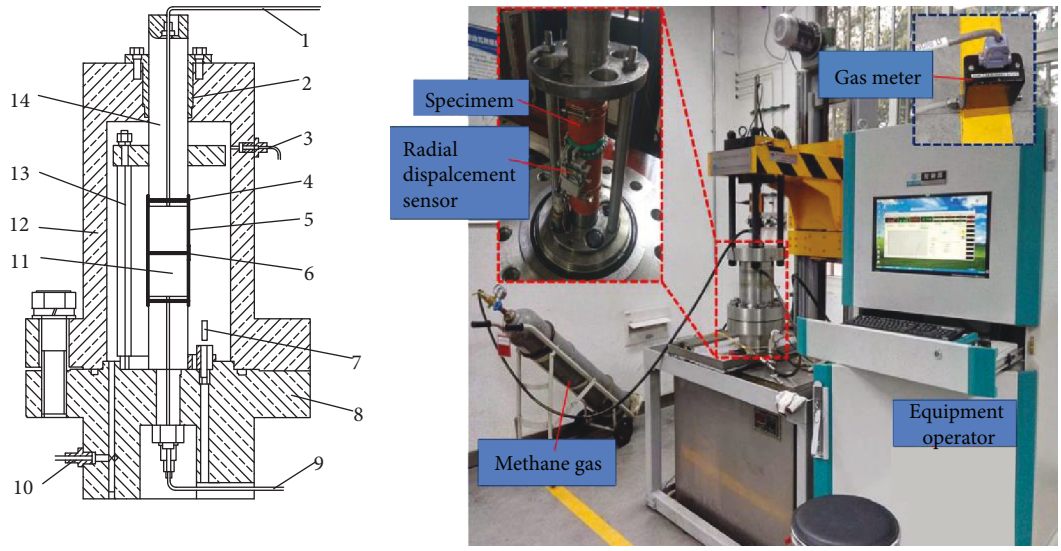

FIGURE 1: Thermal-fluid-solid coupling triaxial servo seepage device. 1: intake tube; 2: guide sleeve; 3: row air tube; 4: metal hoop; 5: heat shrinkable tube; 6: radial displacement sensor; 7: sensor junction column; 8: lower seat; 9: outlet pipe; 10: into and out of oil hole; 11: specimen; 12: upper seat; 13: guide device; 14: pressurized piston rod.

fractured rock shows axial compression deformation, radial expansion, and permeability reduction nonlinearly. As the axial stress increases from 2 MPa to 4 MPa, the axial strain of specimen #j_1 increases by 0.054×10^{-2}, the radial strain increases by -0.001×10^{-2}, and the permeability decreases from 21.206 mD to 19.82 mD: the decrement of permeability was 6.53%; the axial strain of sample #j_2 increases by 0.089×10^{-2}, the radial strain increases by -0.001×10^{-2}, and the permeability decreases from 12.582 mD to 11.499 mD: the decrement of permeability was 8.6%; the axial strain of sample #j_3 increases by 0.141×10^{-2}, the radial strain increases by -0.003×10^{-2}, and the permeability decreases from 9.387 mD to 6.303 mD: the decrement was 32.85%.

Subsequently, load axial pressure of 4 MPa, 6 MPa, 8 MPa, 10 MPa, 12 MPa, 14 MPa, 16 MPa, 18 MPa, and 20 MPa at stage, and load confining pressure at stress control loading rate of 0.05 MPa/s to 8.6 MPa, then unload confining stress to 2.0 MPa at the same rate. The fractured rock shows axial compression deformation, radial shrinkage deformation in the load confining pressure process, while the axial deformation is almost invariable, and radial expansion during unload confining pressure.

(1) The first load and unload confining pressure was under 4 MPa axial stress; as the confining stress increases from 2 MPa to 8.6 MPa, the axial strain of the specimen #j_1 increment was 7.41%, the radial strain increases to 0.185×10^{-2}, and the permeability decrement was 58.74%; the axial strain of sample #j_2 decrement was 47.19%, the radial strain increases to 0.202×10^{-2}, and the permeability decrement was 83.53%; the axial strain of sample #j_3 decrement was 55.32%, the radial strain increases to 0.279×10^{-2}, and the permeability decrement was 38.3%. After unloading confining pressure from 8.6 MPa to 2 MPa, the axial strain of sample #j_1 decrement was 3.45%, the radial strain decreases to 36.22%, and the permeability increment was 6.79%; the axial strain of sample #j_2 increment was 68.09%, the radial strain decreases to 22.77%, and the permeability increment was 157.13%; the axial strain of sample #j_3 increment was 90.48%, the radial strain decreases to 25.45%, and the permeability increment was 3.45%. We know that after the first load and unload confining pressure, the permeability recovery rate of sample #j_1 is 44.06%, the permeability recovery rate of sample #j_2 is 42.35%, and the permeability recovery rate of sample #j_3 is 63.83%. The calculation of permeability recovery rate is as follows: the permeability of specimens is 19.82 mD when confining pressure is 2 MPa and axial pressure is 4 MPa in stages. The permeability of the specimens is 8.732 mD after a cyclic loading and unloading (2 MPa → 8.6 MPa → 2 MPa) confining pressure under constant axial pressure of 4 MPa. The permeability recovery rate of the specimen is the permeability under the loading and unloading confining pressure divided by the original permeability

(2) Maintain 2 MPa confining pressure constant and load axial stress from 4 MPa to 6 MPa; the axial strain of the sample #j_1 increment was 112.5%, the radial strain decrement was 3.39%, and the permeability decrement was 7.94%; the axial strain of specimen #j_2 increment was 81.01%, the radial strain decrement was 5.13%, and the permeability increment

was 2.79%; the axial strain of specimen #j_3 increment was 72.5%, the radial strain decrement was 9.62%, and the permeability decrement was 12.32%. Maintain 6 MPa axial pressure constant and second load and unload confining stress; the axial strain of specimen #j_1 increment was 7.56%, the radial strain increment was 8.77%, and the permeability recovery rate was 7.94%; the axial strain of the sample #j_2 increment was 10.49%, the radial increment was 9.46%, and the permeability recovery rate was 81.08%; the axial strain of the sample #j_3 increment was 7.83%, the radial increment was 9.57%, and the permeability recovery rate was 84.6%

(3) Maintain 2 MPa confining pressure constant and load axial stress from 6 MPa to 8 MPa; the axial strain of the sample #j_1 increment was 62.5%, the radial decrement was 5.65%, and the permeability decrement was 6.11%; the axial strain of specimen #j_2 increment was 51.9%, the radial strain decrement was 6.79%, and the permeability increment was 3.33%; the axial strain of specimen #j_3 increment was 41.26%, the radial strain decrement was 15.05%, and the permeability decrement was 9.09%. Maintain 8 MPa axial pressure constant and third load and unload confining stress; the axial strain of specimen #j_1 increment was 9.13%, the radial strain increment was 5.98%, and the permeability recovery rate was 89.13%; the axial strain of the sample #j_2 increment was 4.58%, the radial strain increment was 5.96%, and the permeability recovery rate was 83.86%; the axial strain of the sample #j_3 increment was 3.49%, the radial strain increment was 8.57%, and the permeability recovery rate was 90.01%

(4) Maintain 2 MPa confining pressure constant and load axial stress from 8 MPa to 10 MPa; the axial strain of the sample #j_1 increment was 42.29%, the radial decrement was 8.87%, and the permeability was unchanged; the axial strain of specimen #j_2 increment was 34.46%, the radial strain decrement was 8.13%, and the permeability increment was 3.87%; the axial strain of specimen #j_3 increment was 32.82%, the radial strain decrement was 23.68%, and the permeability decrement was 5.55%. Maintain 10 MPa axial pressure constant and fourth load and unload confining stress; the axial strain of specimen #j_1 increment was 4.33%, the radial strain increment was 4.43%, and the permeability recovery rate was 92.68%; the axial strain of sample #j_2 increment was 2.94%, the radial strain increment was 4.08%, and the permeability recovery rate was 85.19%; the axial strain of the sample #j_3 increment was 2.31%, the radial strain increment was 10.34%, and the permeability recovery rate was 94.12%

(5) Maintain 2 MPa confining pressure constant and load axial stress from 10 MPa to 12 MPa; the axial strain of the sample #j_1 increment was 25.22%, the radial strain decrement was 13.56%, and the permeability increment was 7.89%; the axial strain of specimen #j_2 increment was 22%, the radial strain decrement was 8.5%, and the permeability was unchanged; the axial strain of specimen #j_3 increment was 23.93%, the radial strain decrement was 41.25%, and the permeability decrement was 6.24%. Maintain 12 MPa axial pressure constant and fifth load and unload confining stress; the axial strain of specimen #j_1 increment was 2.61%, the radial strain increment was 2.94%, and the permeability recovery rate was 90.23%; the axial strain of sample #j_2 increment was 2.34%, the radial strain increment was 3.57%, and the permeability recovery rate was 86.95%; the axial strain of sample #j_3 increment was 1.82%, the radial strain increment was 13.83%, and the permeability recovery rate was 93.34%

(6) Maintain 2 MPa confining pressure constant and load axial stress from 12 MPa to 14 MPa; the axial strain of the sample #j_1 increment was 20.55%, the radial strain decrement was 21.91%, and the permeability increment was 10.83%; the axial strain of specimen #j_2 increment was 18.08%, the radial strain decrement was 10.35%, and the permeability was unchanged; the axial strain of specimen #j_3 increment was 23.36%, the radial strain decrement was 82.24%, and the permeability decrement was 7.19%. Maintain 14 MPa axial pressure constant and sixth load and unload confining stress; the axial strain of specimen #j_1 increment was 3.07%, the radial strain increment was 4.88%, and the permeability recovery rate was 90.23%; the axial strain of the sample #j_2 increment was 1.36%, the radial strain increment was 3.08%, and the permeability recovery rate was 89.99%; the axial strain of the sample #j_3 increment was 1.75%, the radial strain increment was 78.95%, and the permeability recovery rate was 92.31%

(7) Maintain 2 MPa confining pressure constant and load axial stress from 14 MPa to 16 MPa, the axial strain of the sample #j_1 increment was 16.17%, the radial decrement was 64.88%, and the permeability increment was 13.5%; the axial strain of specimen #j_2 increment was 14.34%, the radial strain decrement was 11.19%, and the permeability decrement was 11.09%; the axial strain of specimen #j_3 increment was 20.98%, the radial strain decreases to -0.083×10^{-2}, and the permeability was unchanged. Maintain 16 MPa axial pressure constant and seventh load and unload confining pressure; the axial strain of specimen #j_1 increment was 2.56%, the radial strain increment was 5.36%, and the permeability recovery rate was 92.85%; the axial strain of specimen #j_2 increment was 1.34%, the radial strain increment was 2.52%, and the permeability recovery rate was 93.72%; the axial strain of the sample #j_3 increment was 2.38%, the radial strain increment was 16.87%, and the permeability recovery rate was 91.67%

(8) Maintain 2 MPa confining pressure constant and load axial stress from 16 MPa to 18 MPa; the axial strain of the sample #j_1 increment was 14.51%, the radial strain decrement was 77.97%, and the permeability increment was 7.7%; the axial strain of specimen #j_2 increment was 11.72%, the radial strain decrement was 11.48%, and the permeability decrement was 13.31%; the axial strain of specimen #j_3 increment was 21.05%, the radial strain decreases to -0.239×10^{-2}, and the permeability was unchanged. Maintain 18 MPa axial pressure constant and eighth load and unload confining stress; the axial strain of specimen #j_1 increment was 1.63%, the radial strain increment was 30.77%, and the permeability recovery rate was 90.48%; the axial strain of the sample #j_2 increment was 1.62%, the radial increment was 2.78%, and the permeability recovery rate was 84.59%; the axial strain of the sample #j_3 increment was 1.63%, the radial strain increment was 6.7%, and the permeability recovery rate was 90.92%

(9) Maintain 2 MPa confining pressure constant and load axial stress from 18 MPa to 20 MPa; the axial strain of the sample #j_1 increment was 16.35%, the radial strain decreases to -0.069×10^{-2}, and the permeability increment was 7.9%; the axial strain of specimen #j_2 increment was 10.61%, the radial strain decrement was 15.32%, and the permeability decrement was 9.07%; the axial strain of specimen #j_3 increment was 25.14%, the radial strain decreases to -0.516×10^{-2}, and the permeability decrement was 9.99%. Maintain 20 MPa axial stress constant and ninth load and unload confining stress; the axial strain of specimen #j_1 increment was 3.69%, the radial strain increment was 13.04%, and the permeability recovery rate was 92.68%; the axial strain of the sample #j_2 increment was 1.71%, the radial increment was 3.19%, and the permeability recovery rate was 90.02%; the axial strain of the sample #j_3 increment was 1.89%, the radial strain increment was 1.94%, and the permeability recovery rate was 90.92%

Subsequently, maintain 2 MPa confining pressure constant and increase axial stress until the fractured rock failure; the ultimate strength of specimen #j_1 is 22.15 MPa, the ultimate bearing capacity of sample #j_1 was 22.15 MPa, and the corresponding values of axial strain, radial strain, and permeability were 1.711×10^{-2}, -0.962×10^{-2}, and 5.683 mD, respectively; the ultimate bearing capacity of sample #j_2 was 31.94 MPa and the corresponding values for axial strain, radial strain, and permeability were 1.563×10^{-2}, -0.693×10^{-2}, and 0.676 mD, respectively; the ultimate bearing capacity of sample #j_3 was 22 MPa and the corresponding values for axial strain, radial strain, and permeability were 2.4×10^{-2}, -2.37×10^{-2}, and 1.475 mD, respectively. In summary, it can be seen that in maintain 2 MPa confining stress and the load axial stress process, the pores and cracks of the sample are slowly closed and compacted; the specimen shows axial compression deformation and radial expansion. As the axial pressure level increases, the axial strain increases slowly, and its increment decreases gradually; the radial strain increases slowly and increases negatively, and its decrement increases gradually; the permeability of samples #j_1 and #j_3 from gradually decreasing increases; the permeability of sample #j_2 is the opposite. Because of the anisotropy of the fractured rock and the existence of cracks in the sample, the permeability variation trend is different under different stress states.

During the process constant confining pressure and load axial stress from 8 MPa to 10 MPa, the permeability of sample j_1 was unchanged; this is because the specimen itself is the specimen after triaxial compression failure; it is a fractured rock sample. Then, the permeation characteristic tests of step-by-step axial compression and cyclic loading and unloading confining pressure were carried out. Perhaps, it is the internal pores and cracks of specimens that have been closed after loading to the 8 MPa level under axial pressure. At this time, constant axial pressure and cyclic loading-unloading confining pressure tests are carried out, which makes the internal pores and cracks of the specimen close further during the loading confining pressure process, while the unloading confining pressure fails to make the internal voids and cracks open effectively, resulting in no change in the permeability of specimen j_1 during the next stage of the loading confining pressure process, while the permeability of samples j_2 and j_3 changes. The sample itself is heterogeneous anisotropy, which results in the greater dispersion of the test results. The smaller loading range of the axial compression during the stage loading process is also one of the reasons for the unchanged permeability of sample j_1.

During the load confining stress process, the pores and cracks of the specimen are gradually compacted, and the specimen shows the axial compression deformation and radial compression, leading to reducing the difficulty of passage through the specimen; the permeability gradually decreased. But during the unload confining pressure process, the pores and cracks of the sample gradually open, and the sample shows the axial compression deformation and radial compression, leading to increasing the difficulty of passage through the specimen; the permeability of the specimen increases nonlinearly.The deviatoric stress-strain-permeability curves of specimens did not coincide during the load and unload confining pressure process, and the samples were damaged in a certain degree; therefore, the permeability cannot be restored to the permeability value at loading time, and the permeability recovery degree of samples was different under different axial stress states.

The axial strain, radial strain, and permeability of samples under different stresses are shown in Table 1.

Based on the test results in Table 1, strain-deviatoric stress-permeability curves of sample #j_1 at different axial stress levels were plotted as shown in Figure 3. Only sample #j_1 was analyzed below.

The volumetric strain-deviatoric stress-permeability curves of specimen #j_1 under different stress states are shown in Figure 3(a). We can see that in maintain confining pressure constant and staged load axial stress process, the volumetric strain increases gradually with the increase of

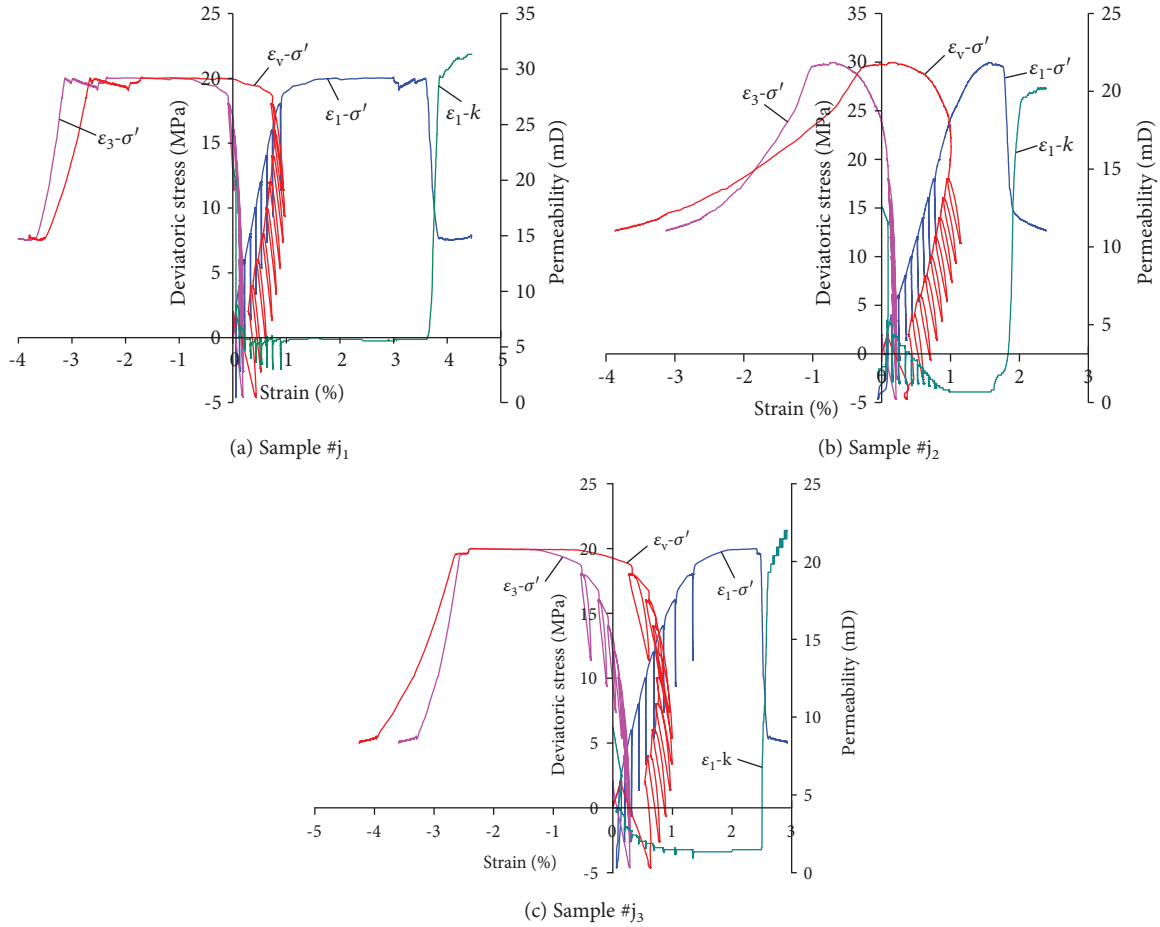

Figure 2: Complete stress-strain-permeability curves of fractured rock.

deviatoric stress, and the permeability was the opposite. But in maintain axial stress constant and unload confining stress process, the volumetric strain of specimens decreases gradually, and permeability was the opposite.

Maintain 2 MPa confining pressure constant and load axial stress 2 MPa → 4 MPa → ⋯20 MPa till the ultimate strength; the strain-deviatoric stress-permeability curves are shown in Figure 3(b). It can be seen that the specimen shows axial compression deformation, radial shrinkage first and then expansion deformation; the axial strain increases gradually, radial strain increases first and then decreases to zero and increases in the negative direction. The relationship of axial strain-deviatoric stress and radial strain-deviatoric stress was subject to the quadratic polynomial function. As the deviatoric stress increases, the permeability decreases nonlinearly, and the decrease amplitude is about 59.44% when the deviatoric stress increases from 2 MPa to 4 MPa, then the decrease amplitude of the permeability decreases slowly and tends to be stable; fitting permeability and deviatoric stress satisfy the exponential function relationship.

Maintain 8.6 MPa confining pressure constant; axial stress is 4 MPa, 6 MPa, …, 20 MPa, respectively; the strain-deviatoric stress-permeability curves are shown in Figure 3(c). We know that the specimen shows axial compression deformation, radial shrinkage first and then expansion deformation. The axial strain increases gradually; fit axial strain and deviatoric stress conform to linear function. The radial strain first increases and then decreases; the maximum radial strain is obtained when the deviatoric stress is -0.6 MPa; the fitting results show that the radial strain and deviatoric stress conform to the quadratic polynomial function. The permeability of the sample decreases nonlinearly, and the slope of permeability-deviatoric stress coincides with exponential function.

When the axial pressure level is 4 MPa, 8 MPa, …, 20 MPa, etc., confining stress decreases from 8.6 MPa to 2 MPa; the deviatoric stress-permeability curves are shown in Figure 3(d). We know that there is axial compression deformation, radial compression first and then expansion. The axial strain increases gradually, and fit axial strain and deviatoric stress are in a linear relationship. The radial strain first increases and then decreases, the radial strain reaches the maximum value when the deviatoric stress is 6 MPa, and then, the radial strain of the sample gradually decreases to zero and increases in the negative direction; fitting radial strain and deviatoric stress are in quadratic polynomial relationship. The permeability of the sample decreases nonlinearly as the deviatoric stress increases; when the deviatoric stress is 14 MPa, the internal crack of the sample opens and the permeability of sample begins to increase; fitting

Table 1: The axial strain, radial strain, and permeability of each sample under different stresses.

σ_1 (MPa)	σ_3 (MPa)	Sample #j_1			Sample #j_2			Sample #j_3		
		ε_1 (%)	ε_3 (%)	k (mD)	ε_1 (%)	ε_3 (%)	k (mD)	ε_1 (%)	ε_3 (%)	k (mD)
2	2	—	—	21.206	—	—	12.582	—	—	9.387
4	2	0.054	-0.001	19.82	0.089	-0.001	11.499	0.141	-0.003	6.303
4	8.6	0.058	0.185	8.177	0.047	0.202	1.894	0.063	0.279	3.889
4	2	0.056	0.118	8.732	0.079	0.156	4.870	0.120	0.208	4.023
6	2	0.119	0.114	8.039	0.143	0.148	5.006	0.207	0.188	3.487
6	8.6	0.128	0.197	6.098	0.163	0.220	1.353	0.195	0.293	2.816
6	2	0.128	0.124	6.791	0.158	0.162	4.059	0.223	0.206	2.950
8	2	0.208	0.117	6.376	0.240	0.151	4.194	0.315	0.175	2.682
8	8.6	0.224	0.199	4.851	0.262	0.223	1.353	0.314	0.286	2.280
8	2	0.227	0.124	5.683	0.251	0.160	3.517	0.326	0.190	2.414
10	2	0.323	0.113	5.683	0.340	0.147	3.653	0.433	0.145	2.280
10	8.6	0.335	0.197	4.019	0.221	0.221	1.218	0.437	0.264	1.878
10	2	0.337	0.118	5.267	0.350	0.153	3.112	0.443	0.160	2.146
12	2	0.422	0.102	5.683	0.427	0.140	3.112	0.549	0.094	2.012
12	8.6	0.435	0.189	3.742	0.448	0.216	1.218	0.555	0.218	1.609
12	2	0.433	0.105	5.128	0.437	0.145	2.706	0.559	0.107	1.878
14	2	0.522	0.082	5.683	0.516	0.130	2.706	0.684	0.019	1.743
14	8.6	0.537	0.173	3.604	0.538	0.207	1.218	0.692	0.150	1.475
14	2	0.538	0.086	5.128	0.523	0.134	2.435	0.696	0.034	1.609
16	2	0.625	0.056	5.821	0.598	0.119	2.165	0.842	-0.083	1.609
16	8.6	0.641	0.149	3.326	0.622	0.198	1.218	0.854	0.047	1.341
16	2	0.641	0.059	5.405	0.606	0.122	2.029	0.860	-0.069	1.475
18	2	0.734	0.013	5.821	0.677	0.108	1.759	1.041	-0.239	1.475
18	8.6	0.744	0.110	3.188	0.701	0.188	1.082	1.053	-0.104	1.207
18	2	0.746	0.017	5.267	0.688	0.111	1.488	1.058	-0.223	1.341
20	2	0.868	-0.069	5.683	0.761	0.094	1.353	1.324	-0.516	1.475
20	8.6	0.898	0.023	3.049	0.790	0.176	0.947	1.343	-0.370	1.207
20	2	0.900	-0.078	5.267	0.774	0.097	1.218	1.349	-0.506	1.341
22/22.15	2	1.711	-0.906	5.683	0.840	0.078	1.082	2.400	-2.370	1.475
24	2				0.906	0.050	0.812			
26	2				0.996	-0.009	0.676			
28	2				1.119	-0.122	0.676			
30	2				1.261	-0.270	0.676			
31.94	2				1.563	-0.693	0.676			

permeability and the deviatoric stress are in accordance with the exponential function.

Based on the test results in Table 1, the strain-deviatoric stress-permeability curves of sample #j_2 and sample #j_3 at different stress levels were plotted as shown in Figures 4 and 5. It can be seen that under different stress levels, the relationship between radial strain and deviatoric stress satisfies the quadratic polynomial function, and the relationship between permeability and deviatoric stress satisfies the exponential function. When the axial pressure is loaded from 2 MPa to 4 MPa, 6 MPa, …, 20 MPa until the ultimate strength, the axial strain and deviatoric stress satisfy the quadratic polynomial relationship. When the axial stress is 4 MPa, 8 MPa, …, 20 MPa, the confining stress is 8.6 MPa or 2.0 MPa; the axial strain-deviatoric stress curves satisfy the linear function relationship.

3.2. Damage Rate of Permeability of Fractured Rock. During the load and unload confining pressure process, the deviatoric stress-permeability curves were not coincident, and the permeability of specimen in the load confining pressure process is higher than the unload confining pressure process. That is, the permeability of the sample was damaged to a certain extent. According to the research results, we used the damage rate of permeability to evaluate the recovery degree of fractured rock permeability, and we used the

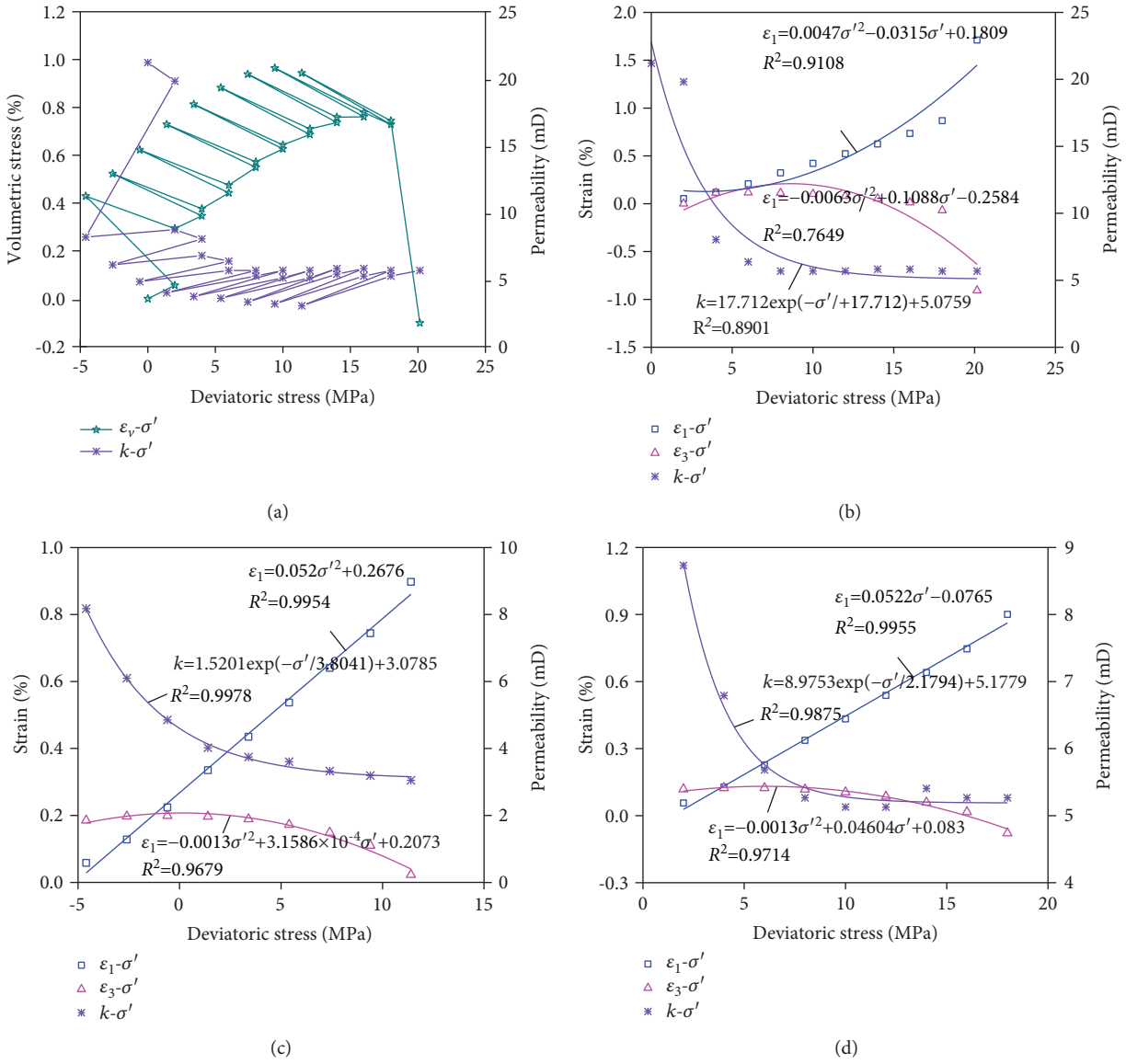

Figure 3: Strain-deviatoric stress-permeability curves of sample #j_1 at different stress levels. (a) Volumetric strain-deviatoric stress-permeability curves; (b) maintain 2 MPa confining pressure, load axial stress (2 MPa → 4 MPa → ⋯20 MPa) at stage; (c) maintain 8.6 MPa confining pressure, axial stress is 4 MPa, 6 MPa, …, 20 MPa, respectively; (d) axial stress levels of 4 MPa, 6 MPa, …, 20 MPa, respectively, unload confining pressure to 2 MPa.

maximum permeability damage rate to evaluate the reduction amplitude of fractured rock permeability [26, 27]. When the permeability damage rate is larger, the recovery degree of permeability is worse; when the maximum permeability damage rate is larger, the reduction amplitude of permeability is greater. The greater the permeability damage rate is, the worse the recovery degree of permeability will be; the greater the maximum permeability damage rate is, the greater the decrease amplitude of permeability will be.

The permeability damage rate d_k can be calculated according to formula (2), and the maximum permeability damage rate $d_{\max}$ can be calculated according to formula (3):

$$d_k = \frac{k_0 - k_1}{k_0} \times 100\%, \tag{2}$$

$$d_{\max} = \frac{k_0 - k_{\min}}{k_0} \times 100\%, \tag{3}$$

where k_1 is fractured rock permeability at the last stress point of unload confining pressure, k_0 is fractured rock permeability at the first stress point of load confining pressure, and $k_{\min}$ is the fractured rock permeability at the maximum stress point.

According to formulas (2) and (3), in the process of load and unload confining pressure, the permeability damage

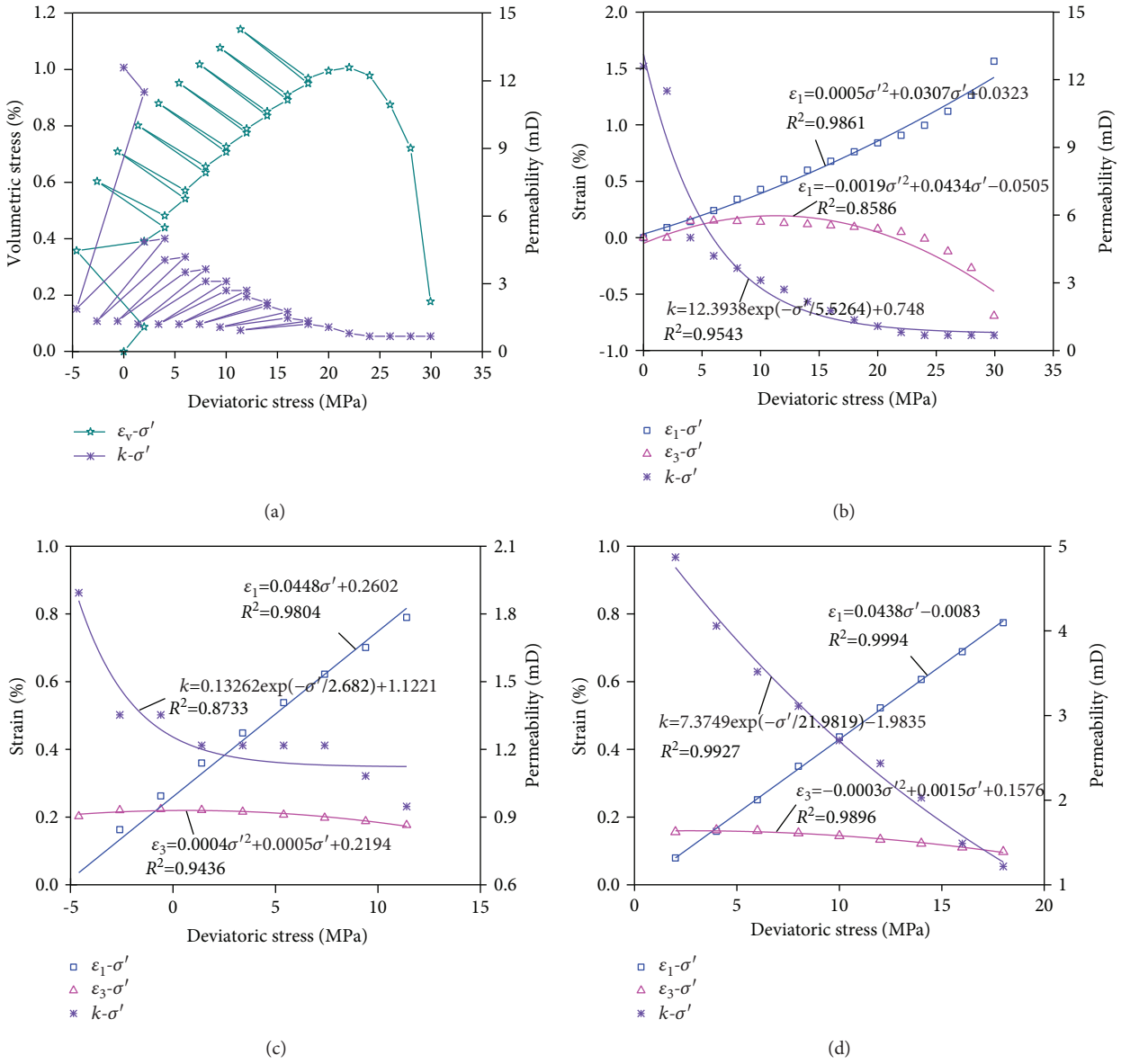

FIGURE 4: Strain-deviatoric stress-permeability curves of sample #j_2 at different stress levels. (a) Volumetric strain-deviatoric stress-permeability curves; (b) maintain 2 MPa confining pressure, load axial stress (2 MPa → 4 MPa → ⋯20 MPa) at stage; (c) maintain 8.6 MPa confining pressure, axial stress is 4 MPa, 6 MPa, …, 20 MPa, respectively; (d) axial stress levels of 4 MPa, 6 MPa, …, 20 MPa, respectively, unload confining pressure to 2 MPa.

rate-axial stress curves and maximum permeability damage rate-axial stress curves of specimens under different axial stresses are shown in Figure 6.

The permeability damage rate-axial stress-maximum permeability damage rate curves of sample #j_1 under different axial pressure levels are shown in Figure 6(a). The results show that d_k is greatest when axial stress is 4 MPa, which indicates that the recovery rate of permeability is the worst after load and unload confining stress under 4 MPa axial stress, and recovery rate is 44.06%. As the axial stress level increases, d_k decreases gradually. When the axial stress is 10 MPa, d_k has the minimum value and then changes in a stable fluctuation. It shows that the permeability recovery degree of sample #j_1 increases gradually with the axial stress level increase, and the recovery degree of permeability tends to be stable when the axial pressure is higher than the stress level of 10 MPa. d_{max} first decreases rapidly and then increases slowly with the increase of the axial stress level, and d_{max} has the maximum value when axial pressure is 4 MPa, which indicates that the permeability reduction degree is the greatest when axial pressure is 4 MPa after load and unload confining pressure. d_{max} has the minimum value when axial stress is 8 MPa, which indicates that the permeability reduction degree is the smallest when the axial stress is 8 MPa. With the axial stress level increase, the permeability reduction degree increases gradually, and

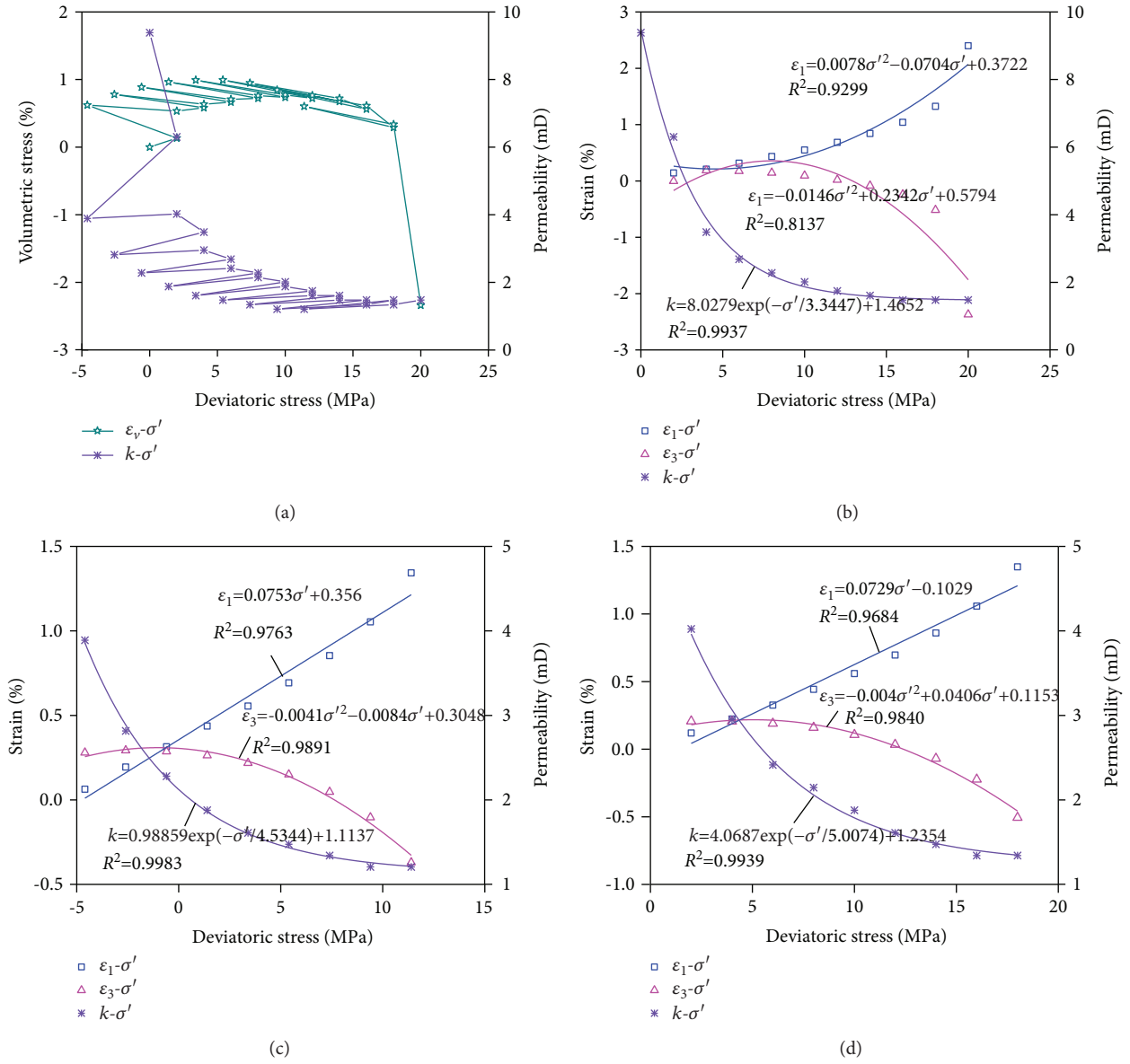

Figure 5: Strain-deviatoric stress-permeability curves of sample #j_3 at different stress levels. (a) Volumetric strain-deviatoric stress-permeability curves; (b) maintain 2 MPa confining pressure, load axial stress (2 MPa → 4 MPa → ⋯20 MPa) at stage; (c) maintain 8.6 MPa confining pressure, axial stress is 4 MPa, 6 MPa, …, 20 MPa, respectively; (d) axial stress levels of 4 MPa, 6 MPa, …, 20 MPa, respectively, unload confining pressure to 2 MPa.

the permeability reduction degree reaches the maximum at the axial stress level of 20 MPa but is lower than that at the initial loading stage.

The permeability damage rate-axial pressure-maximum permeability damage rate curves of specimen #j_2 under different axial pressure levels are shown in Figure 6(b). We know that d_k gradually decreases, and d_k has the minimum value at axial stress of 16 MPa after load and unload confining stress; subsequently, as the axial stress level continue to increase, d_k increases first and then decreases. d_k has the maximum value when the axial stress is 4 MPa, which indicates that the recovery rate of permeability is the worst after load and unload confining stress under axial stress of 4 MPa, and the recovery rate is 42.35%. When axial stress is loaded from a 4 MPa to 6 MPa stress level, the reduction degree of d_k is the greatest after load and unload confining stress; the recovery degree of permeability increases rapidly. With the axial stress level increase, the recovery degree of permeability increases slowly and reaches the maximum value when the axial stress is 16 MPa, then the recovery degree of permeability first decreases and then increases. While d_{max} decreases gradually, d_{max} is almost linear with the axial stress, indicating that the reduction degree of permeability gradually decreases as the axial stress level increases.

The permeability damage rate-axial pressure-maximum permeability damage rate curves of specimen #j_3 under different axial stress levels are shown in Figure 6(c). We know

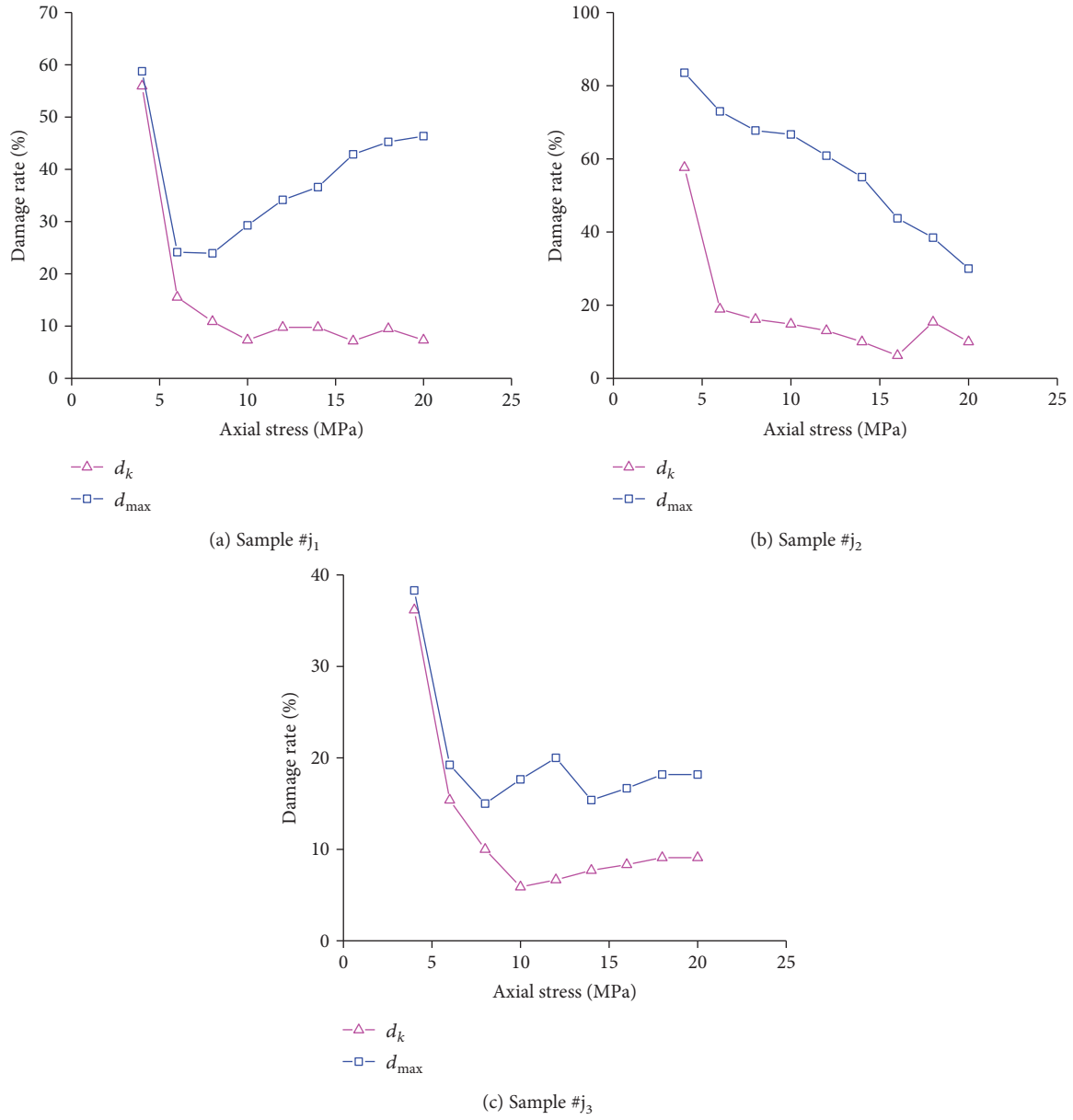

FIGURE 6: Permeability damage rate-axial pressure-maximum permeability damage rate curves of samples during the process of load and unload confining pressure.

that as the axial stress level increases, d_k gradually decreases, and d_k has the minimum value at the axial pressure of 10 MPa. Subsequently, as the increase of the axial stress level continues, d_k increases gradually, which indicates that the recovery rate of permeability is the worst after load and unload confining stress under axial stress of 4 MPa, and the recovery rate is 63.83%. The recovery degree of permeability increases gradually and reaches the maximum value when the axial stress is 10 MPa, then the permeability recovery degree gradually decreases. d_{max} of the sample decreases first, then increases, decreases, and increases the fluctuation of the volatility with the increase of the axial stress level. d_{max} is 38.3% under axial stress of 4 MPa, which indicates that the reduction degree of permeability has the maximum value at axial stress of 4 MPa, and the reduction degree has minimum value at axial stress of 8 MPa. When the axial pressure reaches the stress level of 18 MPa, the reduction degree of the permeability tends to be stable.

Since the permeability of the sample reflects the change of the effective porosity inside the sample, the increase of the permeability reflects the increase of the porosity, and the decrease of the permeability reflects the decrease of the porosity. Therefore, in the load and unload test process, the permeability of the sample has the same change law as the effective porosity. The damage degree of permeability is also reflected in the porosity. After one time load and unload confining stress, the porosity of the sample

is also damaged, and the damage rate is equal to d_k. The sample showed secondary compaction, which is also the reason why the permeability of the sample could not be restored to the initial permeability in the unload confining pressure process under low axial pressure.

3.3. Expansion Rate of Volumetric Strain of Gas-Containing Rock Samples. Under the condition of constant axial pressure, the deviatoric stress-volume strain curves of the specimens do not coincide during load and unload confining stress; the volumetric strain is lower than the unload confining pressure process. That is, after load and unload confining stress, the volume of specimen is subject to a certain degree of expansion and deformation. Therefore, the volume expansion rate and the maximum volume expansion rate of the rock sample can be used to evaluate the expansion degree and the increased amplitude of the rock sample volume. The larger the volume expansion rate of the sample is, the greater the expansion degree of the sample's volume will be; the larger the maximum volume expansion rate is, the larger the increased amplitude of the sample's volume will be.

The volume expansion rate D_{ε_v} can be calculated according to formula (4), and the maximum volume expansion rate $D_{\max}$ can be calculated according to formula (5):

$$D_{\varepsilon_v} = \frac{\varepsilon_{v_1} - \varepsilon_{v_0}}{\varepsilon_{v_0}} \times 100\%, \tag{4}$$

$$D_{\max} = \frac{\varepsilon_{v_{\max}} - \varepsilon_{v_0}}{\varepsilon_{v_0}} \times 100\%, \tag{5}$$

where ε_{v_1} is the volumetric strain at the last stress point of unloading confining stress, ε_{v_0} is the volumetric strain at the first stress point of load confining stress, and $\varepsilon_{v_{\max}}$ is the volumetric strain measured at the maximum stress point.

According to equations (4) and (5), the variation curves of the volume expansion rate and maximum volume expansion rate under different axial stress levels during load and unload confining stress are shown in Figure 7.

The volume expansion rate-axial stress-maximum volume expansion rate variation curves of sample #j_1 during the load and unload confining pressure process are shown in Figure 7(a). It can be seen that the volume expansion rate is about 422.05% at axial stress of 4 MPa after load and unload confining stress, which indicates that the volume expansion degree of the sample is the largest when the axial stress is 4 MPa. The volume expansion rate decreases rapidly to 8.6% when the axial stress reaches 6 MPa and then decreases slowly as the axial stress level increases. The volume expansion rate tends to decrease when the axial stress reaches 12 MPa, that is, the volume expansion degree decreases slowly with the increase of the axial stress level. The maximum volume expansion rate of the specimen has a similar variation with the volume expansion rate. \ When the axial stress reaches 6 MPa, the maximum volume expansion rate decreases rapidly to 50.76%, and then, the increasing degree of volumetric strain decreases slowly.

The volume expansion rate-axial stress-maximum volume expansion rate variation curves of sample #j_2 in the load and unload confining pressure process are shown in Figure 7(b). It can be seen that the volume expansion rate is about 347.27% at axial pressure of 4 MPa, which indicates that the volume expansion degree of the sample is the largest when the axial stress is 4 MPa. The volume expansion rate decreases rapidly to 9.6% when the axial stress reaches 6 MPa and then decreases slowly and tends to be stable as the axial stress level increases. That is, as the axial stress level increases, the volume expansion degree of samples decreases slowly and tends to be stable. The maximum volume expansion rate of the specimen is about 309.12% after load and unload confining stress at axial stress of 4 MPa, which indicates that the volumetric strain is the largest when the axial stress is 4 MPa. The maximum volume expansion rate of the specimen decreases rapidly to 37.36% when the axial stress level reaches 6 MPa, then the volumetric strain increases slowly.

The volume expansion rate-axial stress-maximum volume expansion rate variation curves of sample #j_3 in the load and unload confining stress process are shown in Figure 7(c). It can be seen that the volume expansion rate is about 297.06% at axial stress of 4 MPa, which indicates that the volume expansion degree of the sample is the largest when the axial stress is 4 MPa. The volume expansion rate decreases rapidly to 8.79% when the axial stress reaches 6 MPa and then increases slowly as the axial stress level increases. That is, the volume expansion degree of the specimen is the smallest at the axial stress level of 6 MPa and then increases slowly. The maximum volume expansion rate of the specimen is about 309.12% after load and unload confining stress at axial stress of 4 MPa, which indicates that the increased amplitude of volumetric strain is the largest at axial stress of 4 MPa. When the axial stress level reaches 6 MPa, the maximum volume expansion rate decreases rapidly to 33.88% and then increases slowly, and the curvature increases slowly. That is, the increased amplitude of volumetric strain is the lowest when the axial stress is 6 MPa and then increases gradually as the axial stress level continues to increase.

Since the volumetric strain of the sample reflects the change of the effective porosity inside the sample during the test, the increase of the volumetric strain reflects the increase of the internal porosity of the sample, and the decrease of the volumetric strain reflects the decrease of the internal porosity of the sample. Therefore, in the load and unload test, the volumetric strain of the specimen has the same variation law as the effective porosity, and the volume expansion degree of the sample is also reflected in porosity. After one time load and unload confining stress, the porosity of the specimen is also damaged, and the damage rate is equal to the volume expansion rate. The secondary compaction occurs inside the sample during the test, which is also the reason why the volumetric strain of the specimen cannot be restored to the initial

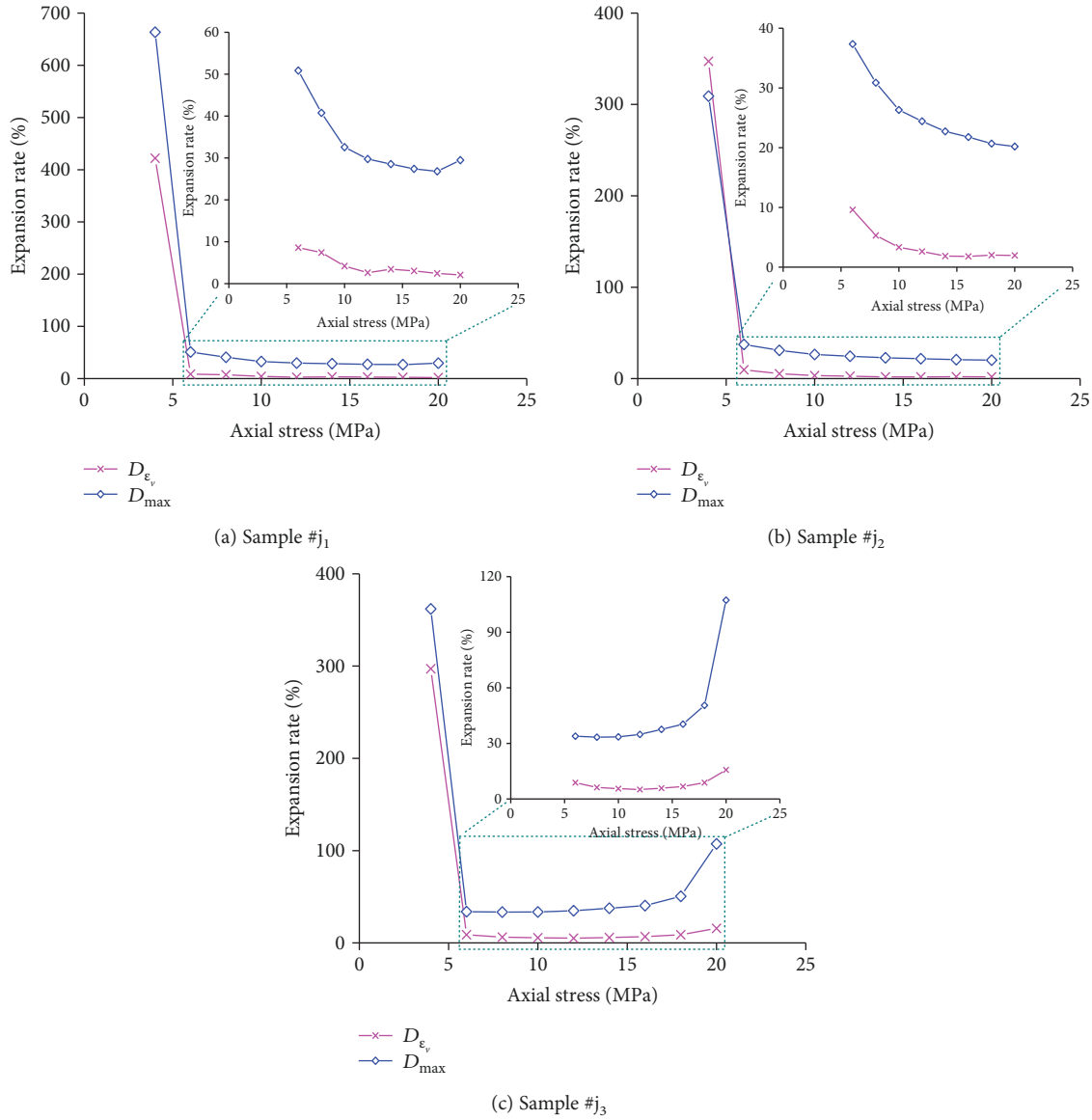

FIGURE 7: Volume expansion rate-axial stress-maximum volume expansion rate variation curves of samples during the process of load and unload confining pressure.

volumetric strain in the unload confining stress process under low axial pressure.

4. Discussion

In the process of coal seam mining, the coal and rock in front of the working face undergo the loading and unloading process, which can be divided into stress reduction area, stress increase area, and original stress area. The process of confining pressure loading can simulate the permeability change law of coal and rock in the stress increase area. During the loading confining pressure process, the axial strain of the specimen is almost constant, and the radial strain increases in the positive direction, which results in the increase of the volumetric strain. Correspondingly, after loading the confining pressure, the increased range of volumetric strain can be expressed by the maximum volumetric expansion rate. In the process of loading confining pressure, the microvoids and cracks in the sample are gradually closed, which makes it more difficult for gas to pass through the sample and reduces the permeability of the sample. Correspondingly, after loading the confining pressure, the decreased range of permeability can be expressed by the maximum permeability damage rate.

The process of unloading confining pressure of the sample can simulate the permeability change law of coal and rock in the stress reduction zone. During the process of unloading confining pressure, the axial strain of the sample is almost constant, the radial direction appears expansion deformed, the radial strain decreases, and the volumetric strain of the

specimen decreases. Correspondingly, the volume expansion degree of the specimen after one loading and unloading confining pressure can be expressed by the volume expansion rate. In the process of unloading confining pressure, the microvoids and cracks in the sample gradually open, which reduces the difficulty of gas passing through the sample and increases the permeability of the sample. Correspondingly, the recovery degree of the permeability of the sample after one loading and unloading confining pressure can be expressed by the permeability damage rate.

5. Conclusion

(1) The relationship between radial strain and deviatoric stress satisfied the quadratic polynomial function, and the relationship between permeability and deviatoric stress satisfied the exponential function under different axial stress levels

(2) In the staged load axial stress process, the axial strain-deviatoric curves of specimens conform to the quadratic polynomial function. The axial strain-deviatoric curves of specimens conform to the linear function when the confining pressure is 8.6 MPa or 2.0 MPa at different axial stress levels

(3) We used the permeability damage rate and maximum permeability damage rate to evaluate the recovery degree and the reduction extent of permeability

(4) We used the volume expansion ratio and the maximum volume expansion ratio to evaluate the expansion degree and increase extent of rock samples' volume

Data Availability

All included experimental data are absolutely reliable, the datasets supporting this article have been uploaded as part of the electronic supplementary material, and the raw data is in Excel format.

Conflicts of Interest

The authors declare that they have no competing interests.

Authors' Contributions

Dongming Zhang and Yushun Yang conceived and designed the experiments; Yushun Yang and Shujian Li performed the experiments and analyzed the data; Yushun Yang wrote the paper. All authors gave final approval for publication.

Acknowledgments

The authors acknowledge the National Science and Technology Major Project of China (2016ZX05045-004).

Supplementary Materials

The original data are the test data monitored by three rock samples during the test. *(Supplementary Materials)*

References

[1] H. M. Zhang, "Experimental on gaseous seepage properties of sandstone in complete stress-strain process," *Journal of China Coal Society*, vol. 34, no. 9, pp. 1063–1066, 2009.

[2] S. Ghabezloo, J. Sulem, S. Guédon, and F. Martineau, "Effective stress law for the permeability of a limestone," *International Journal of Rock Mechanics and Mining Sciences*, vol. 46, no. 2, pp. 297–306, 2009.

[3] D. Ma, X. X. Miao, Z. Q. Chen, and X. B. Mao, "Experimental investigation of seepage properties of fractured rocks under different confining pressures," *Rock Mechanics and Rock Engineering*, vol. 46, no. 5, pp. 1135–1144, 2013.

[4] W. Wei, W. Y. Xu, R. B. Wang, Y. J. Cao, H. L. Wang, and S. R. Feng, "Permeability of dense rock under triaxial compression," *Chinese Journal of Rock Mechanics and Engineering*, vol. 34, no. 1, pp. 40–47, 2015.

[5] W. Wei, Z. Zheng, R. B. Wang, H. L. Wang, and W. Y. Xu, "Experimental study of permeability properties of granitic gneiss under different stress paths," *Chinese Journal of Rock Mechanics and Engineering*, vol. 35, no. 2, pp. 260–267, 2016.

[6] T. Jiang, J. F. Shao, W. Y. Xu, and C. B. Zhou, "Experimental investigation and micromechanical analysis of damage and permeability variation in brittle rocks," *International Journal of Rock Mechanics and Mining Sciences*, vol. 47, no. 5, pp. 703–713, 2010.

[7] R. Zhang, Z. Jiang, Q. Sun, and S. Zhu, "The relationship between the deformation mechanism and permeability on brittle rock," *Natural Hazards*, vol. 66, no. 2, pp. 1179–1187, 2013.

[8] L. Wang, J. F. Liu, J. L. Pei, H. N. Xu, and Y. Bian, "Mechanical and permeability characteristics of rock under hydro-mechanical coupling conditions," *Environmental Earth Sciences*, vol. 73, no. 10, pp. 5987–5996, 2015.

[9] Y. Zhao, Y. Wang, W. Wang, L. Tang, Q. Liu, and G. Cheng, "Modeling of rheological fracture behavior of rock cracks subjected to hydraulic pressure and far field stresses," *Theoretical and Applied Fracture Mechanics*, vol. 101, pp. 59–66, 2019.

[10] W. Xu, R. Wang, W. Wang, Z. Zhang, J. Zhang, and W. Wang, "Creep properties and permeability evolution in triaxial rheological tests of hard rock in dam foundation," *Journal of Central South University*, vol. 19, no. 1, pp. 252–261, 2012.

[11] Z. Liu, J. Shao, S. Xie, and J. Secq, "Gas permeability evolution of clayey rocks in process of compressive creep test," *Materials Letters*, vol. 139, pp. 422–425, 2015.

[12] Z. B. Jiang, A. N. Jiang, H. Li, and S. Y. Wang, "Creep-seepage coupling laws of quartzite under cyclic loading-unloading conditions," *Chinese Journal of Geotechnical Engineering*, vol. 39, no. 10, pp. 1832–1841, 2017.

[13] Q. Kong, H. L. Wang, and W. Y. Xu, "Experimental study on permeability and porosity evolution of sandstone under cyclic loading and unloading," *Chinese Journal of Geotechnical Engineering*, vol. 37, no. 10, pp. 1893–1900, 2015.

[14] C. H. Liang, L. I. Jianfeng, W. A. Chunping, L. I. Jian, S. U. Rui, and W. A. Ju, "Investigation on damage evolution characteristic of granite under compressive stress condition and its impact on permeability," *Chinese Journal of Rock Mechanics and Engineering*, vol. 33, no. 2, pp. 287–295, 2014.

[15] Y. Zhao, Y. Wang, W. Wang, W. Wan, and J. Tang, "Modeling of non-linear rheological behavior of hard rock using triaxial rheological experiment," *International Journal of Rock Mechanics and Mining Sciences*, vol. 93, pp. 66–75, 2017.

[16] L. Wei, Q. Yue-ping, Z. Miao-miao, W. Cui-xia, and W. Ya-ru, "Test study on permeability properties of the sandstone specimen under triaxial stress condition," *Procedia Engineering*, vol. 26, pp. 173–178, 2011.

[17] D. M. Zhang, B. B. Zheng, X. M. Zhang, X. H. Qi, and X. Bai, "Experimental study on the deformation characteristics and permeability laws of gas infiltrated sandstone under unloading confining pressure condition," *Rock and Soil Mechanics*, vol. 38, no. 12, pp. 3475–3490, 2017.

[18] D. M. Zhang, B. B. Zheng, G. Z. Yin, X. M. Zhang, and Y. S. Yang, "Mechanics and permeability characteristics of steep seam roof sandstone under disturbance stress," *Journal of China Coal Society*, vol. 42, no. z1, pp. 128–137, 2017.

[19] F. Huang and B. Hu, "Macro/microbehavior of shale rock under the dynamic impingement of a high-pressure supercritical carbon dioxide jet," *RSC Advances*, vol. 8, no. 66, pp. 38065–38074, 2018.

[20] L. G. Wang, Y. Zhang, X. F. Liu, and Q. Chen, "Experimental research on seepage characteristics of sandstone with single fracture," *Bulletin of the Chinese Ceramic Society*, vol. 37, no. 5, pp. 1804–1811, 2018.

[21] F. Huang, S. Li, Y. Zhao, and Y. Liu, "Study on lateral jetting range during an arc-curved jet impacting nonplanar solid surfaces," *Journal of Fluids Engineering*, vol. 140, no. 10, pp. 101201–101211, 2018.

[22] L. He, Q. Yin, and H. Jing, "Laboratory investigation of granite permeability after high-temperature exposure," *Processes*, vol. 6, no. 4, p. 36, 2018.

[23] F. F. Menezes, "Anisotropy of volume change and permeability evolution of hard sandstones under triaxial stress conditions," *Journal of Petroleum Science and Engineering*, vol. 174, pp. 921–939, 2019.

[24] Y. Zhao, L. Zhang, W. Wang, J. Tang, H. Lin, and W. Wan, "Transient pulse test and morphological analysis of single rock fractures," *International Journal of Rock Mechanics and Mining Sciences*, vol. 91, pp. 139–154, 2017.

[25] P. F. Shan and X. P. Lai, "Numerical simulation of the fluid–solid coupling process during the failure of a fractured coal–rock mass based on the regional geostress," *Transport in Porous Media*, vol. 124, no. 3, pp. 1061–1079, 2018.

[26] M. X. Jing and X. L. Yuan, "Experimental research on core stress sensitivity of carbonate rock," *Natural Gas Industry*, vol. 22, no. z1, pp. 114–117, 2002.

[27] D. K. Wang, J. P. Wei, and G. Z. Yin, "Investigation on change rule of permeability of coal containing gas under complex stress paths," *Chinese Journal of Rock Mechanics & Engineering*, vol. 31, no. 2, pp. 303–310, 2012.